The Formation of Automated Fibre Placement Imperfections and their Growth Using a Tabletop AFP Simulator

Ryan Pederson[1], Reece Haberstock[1*], Nima Bakhshi[2], Adam T Clare[1] and Anoush Poursartip[1,2]

[1] Composites Research Network, Departments of Materials Engineering and Mechanical Engineering, The University of British Columbia, Vancouver, BC, Canada,

[2] Convergent Manufacturing Technologies, Vancouver, BC, Canada

* *Reece.haberstock@composites.ubc.ca*

Keywords: *Automated Fibre Placement; Tow Steering; Wrinkling; Imaging*

1. Abstract

The full potential of automated fibre placement is limited by the formation of defects during the deposition process. Using a tabletop AFP simulator (µAFP) equipped with multi-angle imaging capabilities, this study investigates the mechanisms of how these defects initiate and evolve. Building on our previous research that classified wrinkles into folded wrinkles (initiation through pre-compaction buckling) and unfolded wrinkles (initiated post-compaction), we present quantitative measurements detailing how these defects grow over time. It is observed that both folded and unfolded wrinkles exhibit similar growth trends, with the material tack appearing to be a primary factor influencing the overall defect growth.

2. Introduction

2.1. Motivation and Literature Review

Although automated fibre placement (AFP) is extensively used for manufacturing large composite parts, its full potential remains limited by the formation of process-induced imperfections. This propensity for defects is particularly evident when the tow is steered in-plane or traversed over complex tooling. During a steered deposition, the tow is forced along a curved path, subjecting the outer edge to tension and the inner edge to compression. Since carbon fibres are rigid and essentially inextensible, they cannot compress to accommodate the path geometry. This causes the inside edge to accumulate an excess in length, causing the formation of out-of-plane wrinkles [1].

The resistance to the growth of these defects is solely dependent on the adhesion that is generated between the prepreg tow and the substrate, which is referred to as 'tack'. Defects begin to grow once the residual stress, developed during steered deposition, and its associated strain energy release rate exceed the materials Energy of Separation (EOS) or tack that initially held the tow down [2]. The EOS is viscoelastic, and a defect will grow increasingly more slowly as the available stored stress/energy decreases and thus the energy release rate is reduced. The tack model approach and results indicate that the EOS is a function of deposition rate, which determines the degree of intimate contact, and the peel rate which brings in the viscoelastic nature of the interface decohesion process. As long as full intimate contact is achieved, then tack is insensitive to deposition rate for a given peel rate [2].

Rajan *et al* [3] presented finite element analysis which explicitly included the effects of the tow guide and feed setup on pre-nip buckling. Our own previous work [4], [5] has corroborated these results in showing that the ability or propensity of the tow to buckle prior to the nip point can result in folded wrinkles.

There are several studies that model the formation of wrinkling as an orthotropic plate on an elastic foundation [6] or on a viscoelastic foundation [7]. It is assumed in these methods that the prepreg is initially deposited successfully, with defects appearing after consolidation due to the steering induced stress overcoming the tack between the substrate and the deposited tow.

In previous work [5], we demonstrated that wrinkles can be classified into two categories: folded wrinkles which initiate via buckling prior to compaction, and unfolded wrinkles, which initiate post-compaction without pre-nip buckling. Building upon that foundation, this paper summarizes those initial findings and presents new insights into how these wrinkles grow over time.

2.2. The µAFP System

The steered deposition experiments in this work were conducted using a custom-built AFP simulator dubbed the µAFP, as shown in Figure 1. The µAFP is a gantry system that can produce curvilinear paths at velocities up to 700 mm/s, with a radius as low as 450 mm, and a continuously heated substrate up to 60°C. Additionally, it offers the advantage of having clear and close access to the deposition head. This enables comprehensive video imaging (ahead, behind, and to the side of the roller; as well as overhead and side views of the deposited tow) to study the formation of imperfections, both prior to the nip point and after deposition. The µAFP can deposit a single tow at a time in various positions across the width of the roller. Additional details regarding the mechanical design and control architecture of the system have been previously presented in [4], [5], [8], [9].

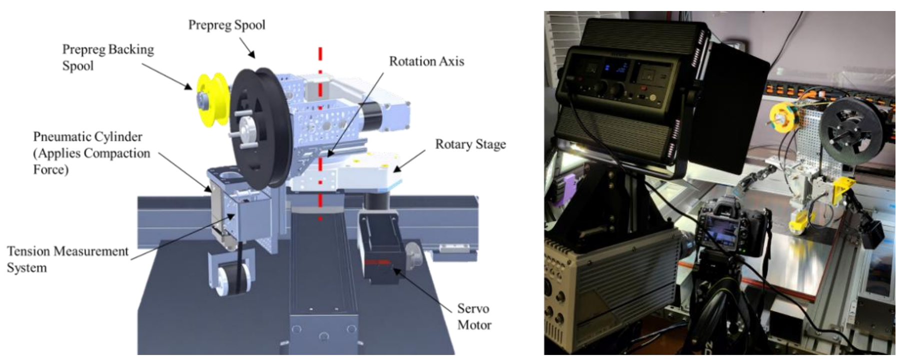

Figure 1. The µAFP system used to conduct the steered deposition experiments in this work. The µAFP system is a 2-axis gantry system equipped with a rotating dispenser head used to perform both in-situ tack tests and steering tests. (Figure adapted from [4], [5])

2.3. µAFP Video Capture

The formation mechanism of the imperfections and their subsequent growth after deposition is captured using several video cameras. As previously shown in [4], [5], the deposition head is instrumented with two 3840 x 2160 (4k) pixel cameras, focused in front and behind the roller. External to the µAFP, a 1920 x 1080 pixel camera is used to capture the side view of the whole test and a high-speed camera, capable of capturing 1024 x 512 pixels at 500 frames per second, can be positioned to focus on desired regions.

Figure 2 highlights the different perspectives that are captured from each of these views. The front view camera, Figure 2-c, is positioned in front of the compaction roller and captures the formation of defects prior to the nip point. The defects that form prior to the nip point are then captured immediately after the compaction roller, Figure 2-a, with the rear camera. The entire test procedure and the growth of the defects are captured using the external side view camera shown in Figure 2-d.

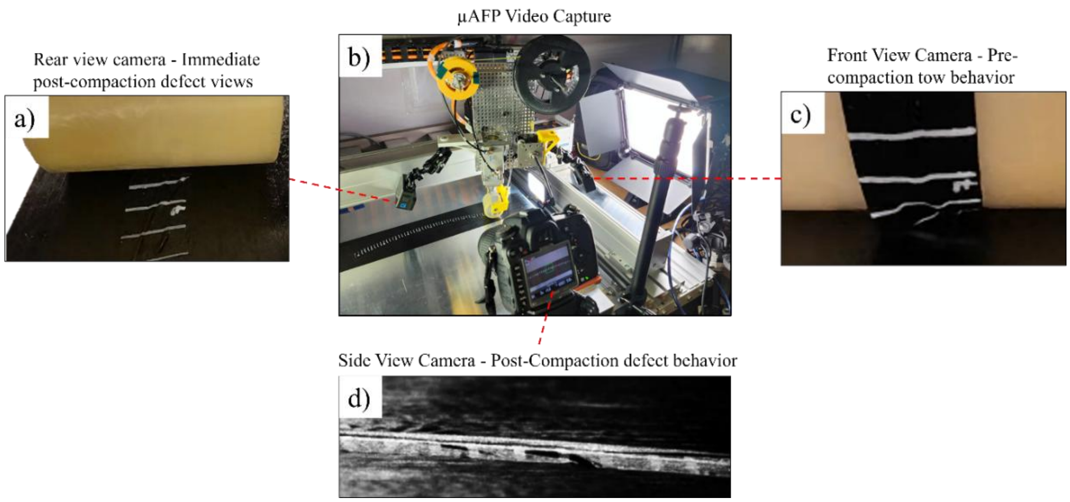

Figure 2. (b) The µAFP system equipped with multiple cameras to capture the tow behavior during the deposition. The view seen in (c) shows the tow behavior just ahead of the roller nip point. The view in (a) shows the tow behavior immediately after initial compaction. (d) shows the side view of the deposition which allows for post deposition defect growth to be studied. (Figure adapted from [4], [5])

3. Material Preparation

The materials used in this study consisted of carbon fibre reinforced polymer (CFRP) prepreg strips measuring 12.7 mm (1/2 in) in width, cut from a bulk roll of Hexcel AS4-8552 (Hexcel, USA) unidirectional prepreg. Each strip was cut to a length of 85 cm, in which 30 cm of the tow is deposited, and the remaining is fed through the µAFP system. The substrate material was prepared in the same way, cutting from a bulk roll of the same prepreg. To improve observation and tracking of the tow deformation, transverse lines were marked on the material before it was laid down. As illustrated in Figure 3, these lines were drawn and numbered on both sides of the tow at 6.35 mm (1/4 in) intervals, enabling deformation features to be identified and synchronized when viewed from both the front and back.

For all tests presented here, the tack or EOS can be considered constant and of the order of 500-700 J/m^2 for the case of the CFRP substrate [8], and substantially lower, of the order of 10 J/m^2, for the aluminum substrate [8], [10].

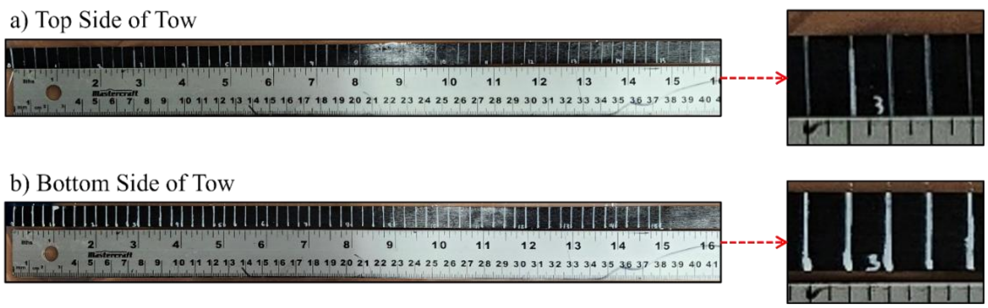

Figure 3. Transverse lines drawn on both (a): the top side of the tow, and (b): the bottom side of the tow. (Figure adapted from [5])

4. Results

4.1. Folded Wrinkle Formation

The formation of a folded wrinkle is a direct result of the pre-compaction behaviour of the prepreg tow as it is fed into the roller nip-point. The test shown in Figure 4 utilizes a 12.7 mm (1/2 in) wide tow deposited onto a 40°C CFRP substrate, with a 250 mm/s deposition rate, a 500 mm steering radius, and 100 N of compaction force applied with a compliant roller. In Figure 4-a, the front-view roller camera shows the tow buckling right before it reaches the roller nip-point. Once consolidated under the roller, this buckle in the tow cannot be flattened out, which creates a permanent fold in the tow behind the roller. Figure 4-b confirms that the buckled section ahead of the roller turned into a folded wrinkle behind the roller. After initial consolidation, the wrinkle begins to lift off, increasing in height and width over time. Figure 4-c shows the state of the wrinkle after 1200 seconds, showing that the wrinkle continued to grow after the layup was completed.

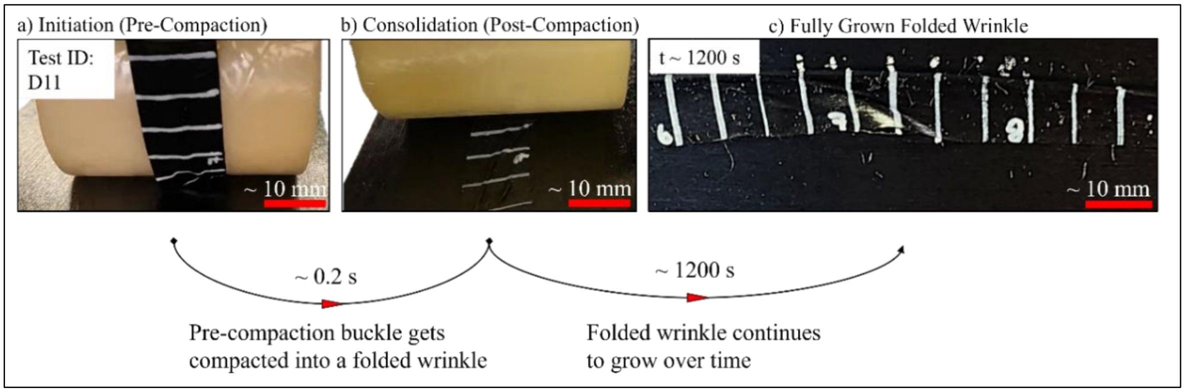

Figure 4. The formation sequence of a folded wrinkle. a) the tow buckles immediately ahead of the roller nip-point. b) the pre-compaction buckle gets compacted into a folded wrinkle. c) the folded wrinkle after 1200 seconds of developnment. (Figure adapted from [4], [5])

4.2. Unfolded Wrinkle Formation

In contrast to folded wrinkle formation, an unfolded wrinkle develops through a different sequence of events that does not involve pre-nip buckling ahead of compaction. Figure 5 uses a 12.7 mm (1/2 in) wide tow deposited onto a 40°C CFRP substrate, with a 250 mm/s deposition rate, a 500 mm steering radius, and 100 N of compaction force applied with a compliant roller. As shown in Figure 5-a, the front-view camera does not reveal any pre-nip buckling ahead of the roller, and the tow is successfully laid down flat without any folding or lift off behind the roller, as seen in Figure 5-b. Despite no defect being present initially, lift off begins to occur after approximately 60 seconds. As shown in Figure 5-c, the tow eventually lifts off the substrate at the inner compression edge. This indicates that the defect likely occurs due to steering induced stresses overcoming the tack, allowing the material to begin lifting from the substrate. Similar to the folded wrinkle, the unfolded wrinkle also continues to grow in height and width over time, taking about 1200 seconds to become fully developed.

Figure 5-c also captures tow pull-up and longitudinal splitting at the outer tension edge. It is important to note that these specific tension edge defects are excluded from the current analysis, as they appear to form independently of the wrinkles and are far enough away that their effects on subsequent wrinkle growth are currently ignored.

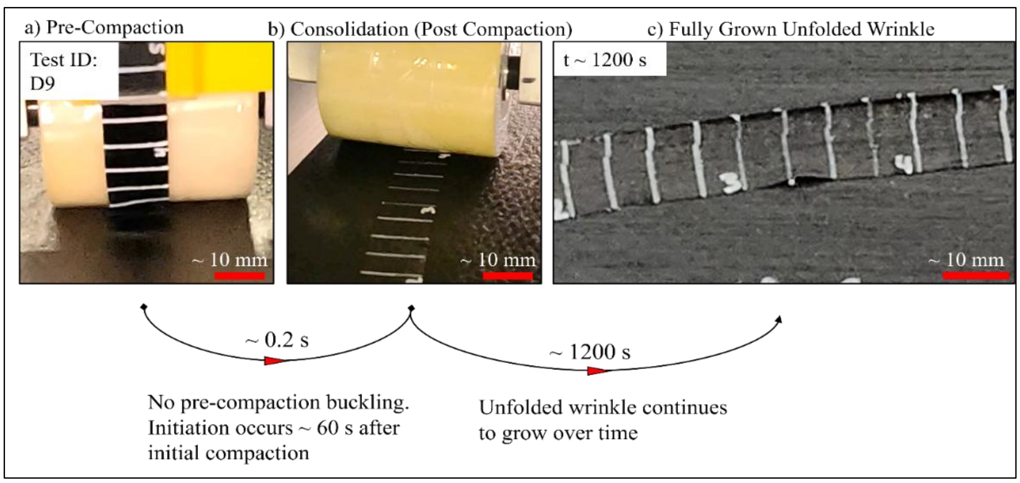

Figure 5. The formation sequence of an unfolded wrinkle. a) Ahead of the roller nip-point, no pre-nip buckling is visible. b) immediately after compaction, no defect is visible until 60 seconds later. c) the fully grown unfolded wrinkle after 1200 seconds of growth time (Figure adapted from [4], [5])

4.3. Folded Wrinkle Growth on a CFRP Substrate

We first present a steering test conducted using a CFRP substrate. Figure 6 and Figure 7 are stills from this test, which use a 12.7 mm (1/2 in) wide tow deposited at a substrate temperature of 40°C, with a 50 mm/s deposition rate, a 500 mm steering radius, and 100 N of compaction force applied with a compliant roller. While multiple folded wrinkles formed during this test, the growth of the specific folded wrinkle circled in red (Figure 6) was isolated for analysis. Figure 7 provides stills from the captured video, illustrating how the wrinkle progressed over a time of 1200 seconds. To quantify the growth of the wrinkle, the video was used to generate the wrinkle growth plots presented in Figure 8. These include wrinkle height vs time, growth rate vs time, and growth rate vs wrinkle height. It can be seen that the wrinkle exhibits very fast initial growth, with the rate levelling off over time. Additionally, the growth rate appears to decrease roughly linearly with the wrinkle height.

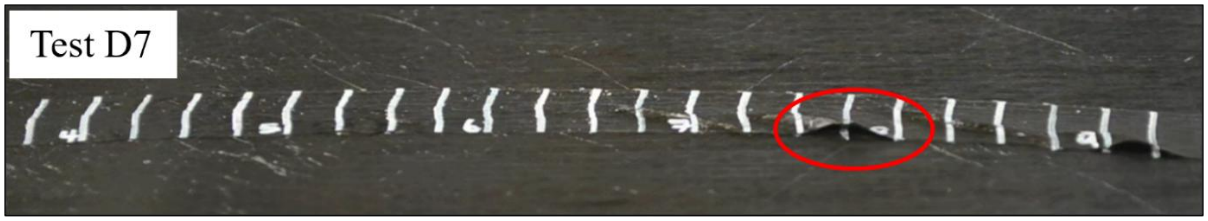

Figure 6. The folded wrinkle being measured in Figure 8. This test was conducted at a steering radius of 500 mm, a 40° C CFRP substrate, 50 mm/s deposition rate, and 100 N of compaction force applied with a compliant roller.

a) t = 0 s b) t = 60 s c) t = 120 s d) t = 300 s e) t = 1200 s

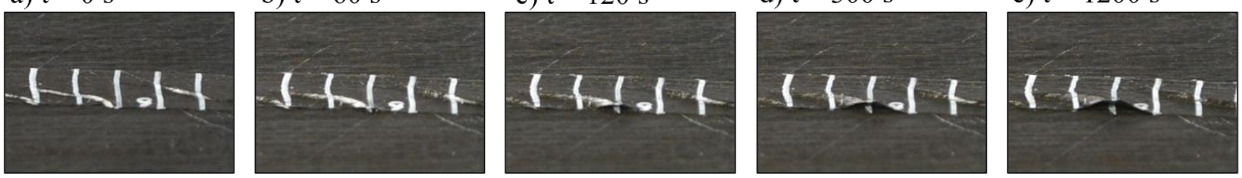

Figure 7. The side view camera image sequence shows the growth of the folded wrinkle from Figure 6 over a time of 1200 seconds.

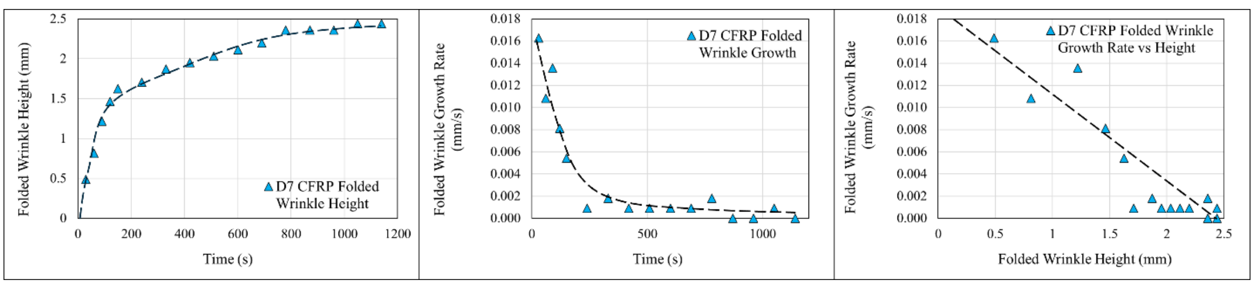

Figure 8. Folded wrinkle growth behaviour for test shown in Figure 6 and Figure 7. The left panel shows the folded wrinkle height over time, the middle panel shows the folded wrinkle growth rate over time, and the right panel shows the folded wrinkle growth rate as a function of folded wrinkle height.

4.4. Folded Wrinkle Growth on an Aluminum substrate

To isolate the influence of substrate material and its associated tack on folded wrinkle growth, a comparative steering test was conducted on an aluminum substrate. Figure 9 and Figure 10 are still images from this deposition, where a 12.7 mm (1/2 in) wide tow was deposited onto a 40°C aluminum substrate, a deposition rate of 700 mm/s, a steering radius of 450 mm, and with a 100 N of applied compaction force via a compliant roller. Although the folded wrinkle initiated in a manner similar to the CFRP substrate test, its subsequent propagation occurred over a span of seconds rather than minutes. Figure 11 shows the growth of the defect stabilizing after 1.5 seconds, representing an approximate 1000 times increase in growth rate on the aluminum substrate relative to the CFRP baseline.

This drastically faster defect propagation is primarily driven by the substantial difference in tack developed between the two different substrate types. The aluminum substrate exhibits a significantly lower tack (~10 J/m^2) compared to the CFRP substrate (500 – 700 J/m^2) [8], [10], allowing the resulting folded wrinkle to grow much quicker. It is important to note that the aluminum deposition also utilized a tighter steering radius (450 mm vs. 500 mm), and an elevated deposition rate (700 mm/s vs. 50 mm/s). However, the combined effect of these variations is minor relative to the large reduction in tack.

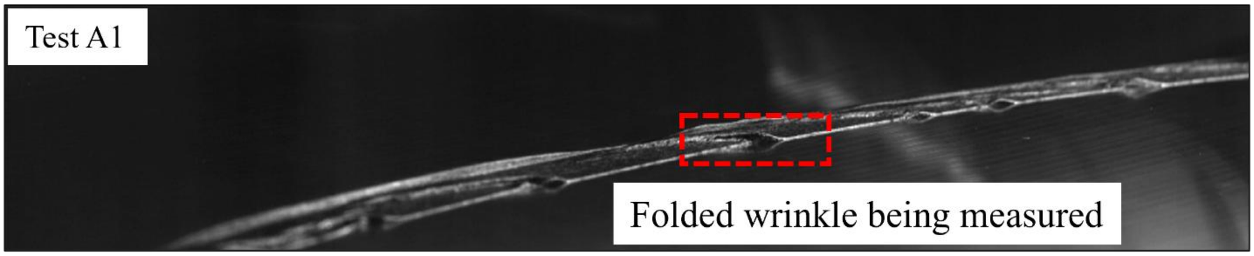

Figure 9. The folded wrinkle being measured in Figure 10. This test was conducted at a steering radius of 450 mm, a 40° C aluminum substrate, 700 mm/s deposition rate, and 100 N of compaction force applied with a compliant roller.

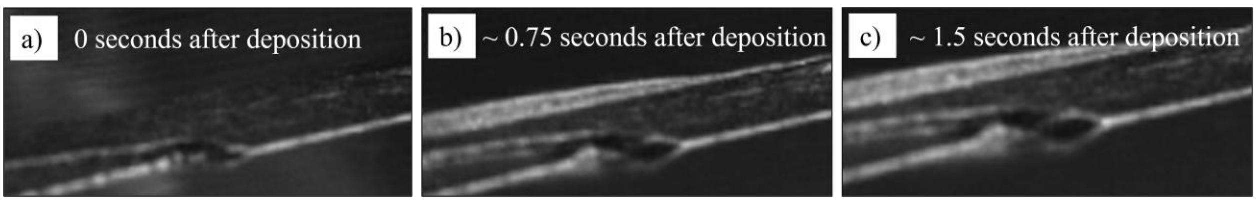

Figure 10. The side view camera image sequence showing the growth of the folded wrinkle from Figure 9 over a time of 1.5 seconds.

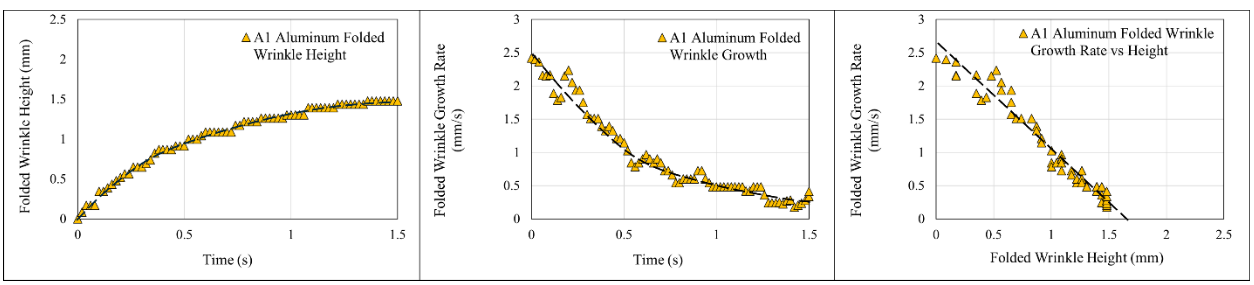

Figure 11. Folded wrinkle growth behaviour for test shown in Figure 9 and Figure 10. The left panel shows the folded wrinkle height over time, the middle panel shows the folded wrinkle growth rate over time, and the right panel shows the folded wrinkle growth rate as a function of folded wrinkle height.

4.5. Unfolded Wrinkle Growth on a CFRP Substrate

To evaluate the behaviour of unfolded wrinkles, a deposition test (previously introduced in Figure 5) was conducted using a 12.7 mm (1/2 in) wide tow deposited onto a 40°C CFRP substrate, a deposition rate of 250 mm/s, a steering radius of 500 mm, and with 100 N of compaction force applied with a compliant roller. Figure 12 highlights the specific defect being measured, and Figure 13 provides sequential images of its development. Unlike folded wrinkles, the unfolded wrinkle exhibits a delayed initiation, with liftoff occurring post-compaction. The tow is initially fully consolidated and begins to lift off after approximately 60 seconds.

Following the delayed onset, the growth of the unfolded wrinkle was quantified in Figure 14. The wrinkle exhibits a rapid initial growth with gradual plateauing over time. This growth pattern is highly similar to the previously measured folded wrinkles (Figure 8, Figure 11). Furthermore, because this test utilized the CFRP substrate, the defect grew over a comparable timeline to the CFRP folded wrinkle, reinforcing that the substrate's tack governs the time required for stabilization.

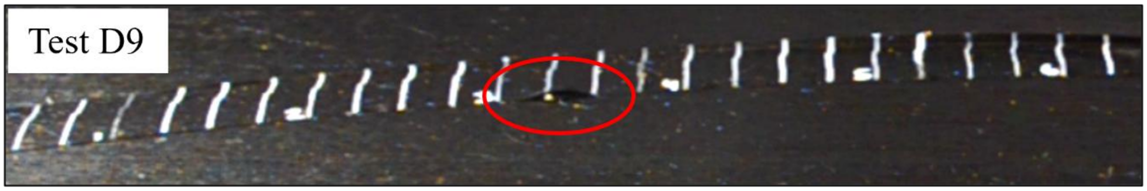

Figure 12. The final height of the unfolded wrinkle being measured. This test was conducted at a steering radius of 500 mm, a 40° C CFRP substrate, 250 mm/s deposition rate, and 100 N of compaction force applied with a compliant roller.

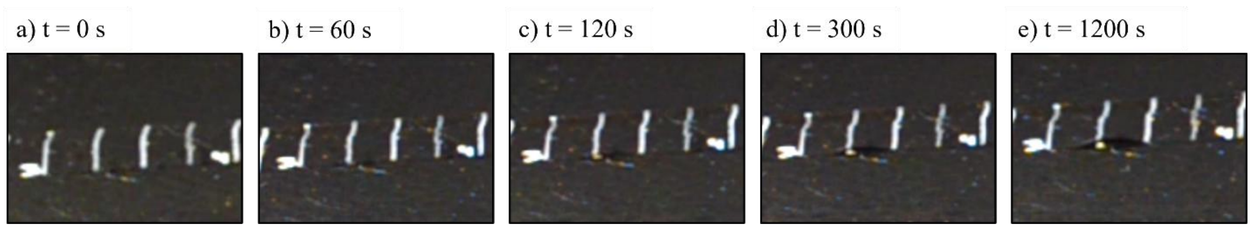

Figure 13. Side view camera image sequence showing growth of the unfolded wrinkle from Figure 12, over a timeframe of 1200 seconds.

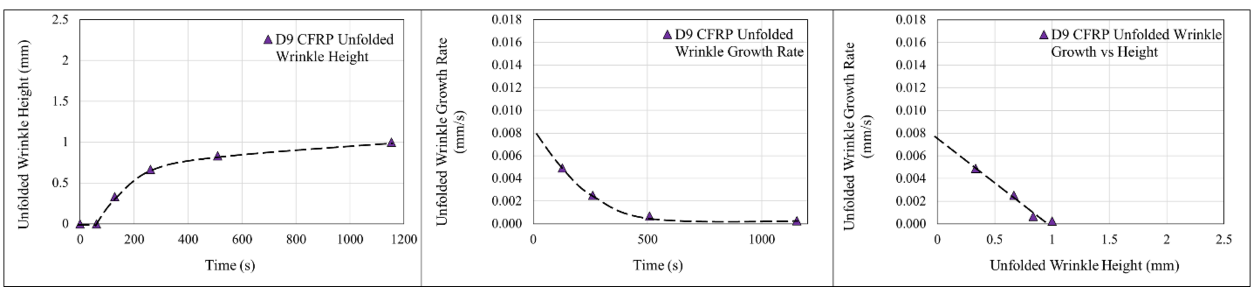

Figure 14. Unfolded wrinkle growth behaviour for the test presented in Figure 12 and Figure 13. The left panel shows the unfolded wrinkle height over time, the middle panel shows the unfolded wrinkle growth rate over time, and the right panel shows the unfolded wrinkle growth rate as a function of unfolded wrinkle height.

5. Discussion

This study identifies distinct initiation behaviours for folded and unfolded wrinkles during the AFP deposition process. While both defect types originate from excess length in the material due to steering, their formation follows a different sequence of events. Folded wrinkles initiate through buckling ahead of the roller nip-point, and unfolded wrinkles initiate post-compaction, forming through a localized lift off where steering-induced stresses overcome the local tack. Thus, folded wrinkles start to grow immediately, unfolded wrinkles have an initiation time before the wrinkle is observable.

Despite their distinct initiation mechanisms, both folded and unfolded wrinkles exhibit similar growth patterns once the defect formed. The substrate type and its associated tack level appear to be the primary factor influencing the growth rate and the time required for the defect to stabilize.

6. Conclusion

Using a tabletop AFP simulator with in-situ cameras, the initiation and growth of folded and unfolded wrinkles was studied. The two defect types are distinct in their formation, where folded wrinkles initiate via pre-nip buckling and unfolded wrinkles have a tack-dependent initiation post-compaction. Both defects grow similarly once formed depending on the substrate's level of tack. These findings suggest that effectively mitigating each defect type requires different strategies. Future work should investigate how additional process parameters influence defect formation and how folded and unfolded wrinkles interact with other AFP defect types such as tow pull-up, in-plane waves, and in-plane shearing.

7. Acknowledgements

The authors would like to acknowledge the financial support of the industrial members of the Composites Research Network (The Boeing Company, Toray CMA, and Convergent) as well as the Canadian Federal Government (NSERC and PacifiCan) as well as many useful conversations with our industrial colleagues.

8. References

[1] R. Harik, C. Saidy, S. J. Williams, Z. Gurdal, and B. Grimsley, "Automated Fiber Placement Defect Identity Cards: Cause, Anticipation, Existence, Significance, and Progression," in *Proceedings of the Society for the Advancement of Material and Process Engineering (SAMPE) Conference and Exhibition*, Diamond Bar, CA, United States, May 2018. Accessed: Jun. 19, 2025. [Online]. Available: https://ntrs.nasa.gov/citations/20200002536

[2] A. Forghani *et al.*, "Experimental Calibration of a Numerical Model of Prepreg Tack for Predicting AFP Process Related Defects," presented at the SAMPE, Diamond Bar, CA, United States, May 2018. Accessed: Jul. 14, 2025. [Online]. Available: https://ntrs.nasa.gov/citations/20200002539

[3] S. Rajan, M. A. Sutton, S. Sockalingam, W. McMakin, Z. Gurdal, and A. Kidane, "Simulations and experiments for automated fiber placement of prepreg slit tape: Wrinkle formation and fundamental observations," *Compos. Part B Eng.*, vol. 201, p. 108287, Nov. 2020, doi: 10.1016/j.compositesb.2020.108287.

[4] R. Pederson, N. Bakhshi, A. Clare, and A. Poursartip, "Investigation of Defect Formation in Automated Fiber Placement Using a Tabletop AFP Simulator," in *Proceedings of the 40th ASC Technical Conference*, Dayton, OH, Oct. 2025.

[5] R. Pederson, N. Bakhshi, A. Clare, and A. Poursartip, "Folded and Unfolded Wrinkle Formation During Steering Using an AFP Tabletop Simulator," in *Proceedings of the Society for the Advancement of Material and Process Engineering (SAMPE) Conference and Exhibition*, Seattle, WA, United States, Apr. 2026.

[6] M. Belhaj and M. Hojjati, "Wrinkle formation during steering in automated fiber placement: Modeling and experimental verification," *J. Reinf. Plast. Compos.*, vol. 37, no. 6, pp. 396–409, Mar. 2018, doi: 10.1177/0731684417752872.

[7] N. Bakhshi and M. Hojjati, "Time-dependent wrinkle formation during tow steering in automated fiber placement," *Compos. Part B Eng.*, vol. 165, pp. 586–593, May 2019, doi: 10.1016/j.compositesb.2019.02.034.
[8] N. Bakhshi, "Investigation of prepreg tack through development of an AFP simulator using in-situ sensing and physics-based simulation," Ph.D Thesis, The University of British Columbia, 2023. doi: 10.14288/1.0438302.
[9] N. Bakhshi, X. Yin, Z. Chen, J. D. W. Madden, and A. Poursartip, "Exploring Science-based Automation Using a Small AFP Demonstrator," in *Proceedings of the Society for the Advancement of Material and Process Engineering (SAMPE) Conference and Exhibition*, Seattle, WA, Apr. 2023. doi: 10.33599/nasampe/s.23.0189.
[10] R. Pederson, "Defect Formation in Automated Fiber Placement using a TableTop AFP Simulator," Master's thesis, in preparation, The University of British Columbia, Vancouver, BC, 2026.